This is the Accepted Manuscript version of a Published Work that appeared in final form in Composites Part B: Engineering 58 : 408-417 (2014) . https://doi.org/10.1016/j.compositesb.2013.10.086

Calibration patterns for predicting residual strengths of steel fibre reinforced concrete (SFRC)

A. Orbe, E. Rojí*, R. Losada, J. Cuadrado

Construction Engineering Area, Department of Mechanical Engineering, Engineering Faculty of Bilbao, University of the Basque Country (UPV/EHU), Alameda Urquijo, s/n, 48013, Bilbao, Spain

Abstract

Steel Fibre Reinforced Concrete (SFRC), a composite construction material, needs reliable prediction and control techniques to promote its use in structural applications. The distribution and orientation of fibres within the concrete matrix plays a major role in the mechanical behaviour of the structural element. Since the observation of those fibres is impossible once the concrete is hardened, new non destructive testing (NDT) techniques have been develop for its analysis. The application of a magnetic field to the concrete, can lead to check the homogeneity of the material based on the different permeability that provide the fibres according to their distribution and orientation. Based on the mentioned magnetic method, an application oriented correlation is established among these last terms on one hand and the mechanical response of the material on the other. The paper proposes a methodology to infer, non-destructively, the spatial dispersion of mechanical properties throughout the structure. The suitability of the method is

*Corresponding author
Email address: eduardo.roji@ehu.es (E. Rojí)

assessed comparing the results with Computational Fluid Dynamics (CFD) simulations.
Keywords: A. Discontinuous reinforcement, B. Magnetic properties, D. Non-destructive testing, D. Mechanical testing, Steel fibre reinforced concrete, Computational Fluid Dynamics (CFD)

1. Introduction

The range of potential applications for cementitious composites is increasing, as knowledge of their properties improves. The tensile behaviour and the durability of Steel Fibre Reinforced Concrete (SRFC) have been widely studied [1] [2] [3] [4] [5]. Correct orientation and uniform distribution of the fibres in the composite must be guaranteed [6] and then verified using appropriate quality control methods, before the material may be approved for construction purposes. Assuming an identical fibre orientation, an uniform distribution of the fibres throughout the wall is necessary to achieved an equal response of the material at every point. The appropriate orientation on the other hand, will be the one that provides greater strength, in the maximum tensile effort directions.

The most direct method of testing fibre amounts is a destructive method, which involves crushing the specimen and then extracting and weighing its fibres. Orientation can be estimated based on image analysis and stereological principles [7] [8] [9], while computer tomography (CT) can accurately display the fibres within the structural element [10] [11]. However, these methods, whether direct or indirect, destructive or non-destructive, are not easily applied to built structures.

New indirect non-destructive techniques have recently been developed that measure the electric resistivity, impedance, permittivity, magnetic permeability, etc. of the finished element, so that the real effects of casting, vibrating and wall-effects are taken into account. The techniques include Waveguide antennae [12], alternate current impedance spectroscopy (AC-IS) [13], electrical resistivity methods [14] and open-ended coaxial probe reflectometry methods [15] among others. Magnetic methods have been proposed as one of the most interesting quality control methods, not only to test fibre orientation, but also to arrive at accurate estimates of distribution. The basis of this method has already been described in UNE 83512-1:2005 Spanish Standard, although it is now no longer valid. However, new research has successfully developed the method [16]. Several researchers [17] [11] have applied this technique and have tested its reliability, economy and simplicity. The same method with a slightly different set-up has also been validated for thin slabs [18] [19] [20]. Obviously, the method is only valid with metallic fibre reinforcements, as only ferromagnetic fibres can alter the magnetic field and cause variations in the measurement of inductance.

The scope of this research focuses on widening the significance of the magnetic methods which from measurement of fibre dispersion can be also used to infer mechanical properties. Several authors have mentioned the correlation between fibre orientation and residual tensile strength [21] [22] [23] [24]. The measured variation of inductance mentioned above can indirectly determine the performance of the specimens in bending tests, thereby obtaining the residual strength of post-cracking behaviour The aim is not to replace the common bending test specified in current regulations (with its

multiple variations). A direct measurement may be more appropriate for a small-scale specimen. However, it is interesting to note the relationship between inductance and strength in cases where specimens are not available, such as for real structural elements.

The flowability of some concretes, such as Self-Compacting Concretes (SCC), is known to force the aleatory orientations of the fibres [25] [26]. A predictive simulation of the casting process, can provide useful information about the flow velocity fields which could be linked to the orientation of fibres. Therefore, the mechanical performance of the material can be also determined for the whole structure. Over the last 3 decades, computational tools have been developed to simulate concrete flow [27]. Diverse research lines, as homogeneous fluid, discrete particles and particles suspended in a viscous medium [28], have been successfully applied. However, few of them have been applied for large size structural elements [29] and only for SCC.

The paper presents the study of a real-scale Steel Fibre Reinforced Self-Compacting Concrete (SFRSCC) wall. The analysis of the structure its for possible applications, requires an exhaustive characterization of the material at different positions within the wall. For this purpose, several specimens, cubic and prismatic, are extracted from the wall and the orientation of the fibres inside is determined. The measurement proportionality of three coils was checked using different measurement equipments, such as portable coils and impedance analysers. Each device was equally effective, except for slight differences in accuracy and precision. Also the goodness of the method is assessed comparing the detected orientations with those predicted by a CFD simulation of the casting process. Although one fibre type was analysed,

similar procedures will be valid for other types. Regardless of the device, the correction factors that are presented allow us to estimate the fibre amount from a calibration pattern. The transformation parameters are used to isolate inductance variation values within the prismatic specimens and to predict their bending and residual strengths.

2. Materials

Our study focuses on the casting of a real-scale, 3-meter high, 6-meter long and 0.15-meter thick structural wall. The specimens under analysis were extracted by cutting them from the wall. The proposed inductive method is only effective with ferromagnetic materials and the concrete mix-design has no influence on inductance variation. However, as preferential fibre orientations are studied in the context of research, a Steel Fibre Reinforced Self-Compacting Concrete (SFRSCC) was designed. The mix-design and fresh state properties are summarised in Table 1 and Table 2, respectively. The self-compactness property causes a flow-induced fibre orientation, that the authors are studying in parallel with Computational Fluid Dynamics (CFD) techniques. The wall was cast by pumping the concrete from the bottom left-hand-side corner, forcing the mass to flow along the formwork, which oriented the fibres in that direction. Those specimens, therefore, presented noticeable orientation differences along the length and height of the wall. Fibre orientation and amount was known to be different and their properties which was in itself a test of the accuracy of the method.

Straight fibres with hooks at each end were used, in order to ensure mechanical anchoring to the concrete matrix. They were 50 mm in length, with

Materials dosage						
Cement (kg/m^3)	Sand (0-4) (kg/m^3)	Gravel (4-11) (kg/m^3)	Plasticizer (l/m^3)	Superplasticizer (l/m^3)	Steel fibres (kg/m^3)	Water (l/m^3)
434	1141	626	4.43	5.02	50	178

Table 1: SFRSCC Mix-design.

	T_{50} (s)	D_f (mm)
Slump flow	1.9	710

Table 2: Fresh properties.

a circular section of 1 mm in diameter. The tensile strength of the drawn wire was 1100 MPa. These fibres comply with EN 14889-1 type 1 (cold-drawn wire) and ASTM A820/A820M-04 type 1 (cold-drawn wire). The average fibre amount in the wall that functions as concrete reinforcement was 50 kg/m^3. In the first part of this study, 75 cubic specimens were tested. The specimens measured approximately 150 x 150 x 150 mm, along each side. The second part was based on the measurements of 7 prismatic specimens (600 mm-long and 150x150 mm-cross section, approx.). Each coil was used to perform tests on concrete at different ages. Finally, based on the data acquired in the preceding steps, the Limit of Proportionality (LOP) values and successive residual strengths ($f_{R,i}$) were predicted for 11 different prismatic specimens. Figure 1 illustrates the position of all the specimens.

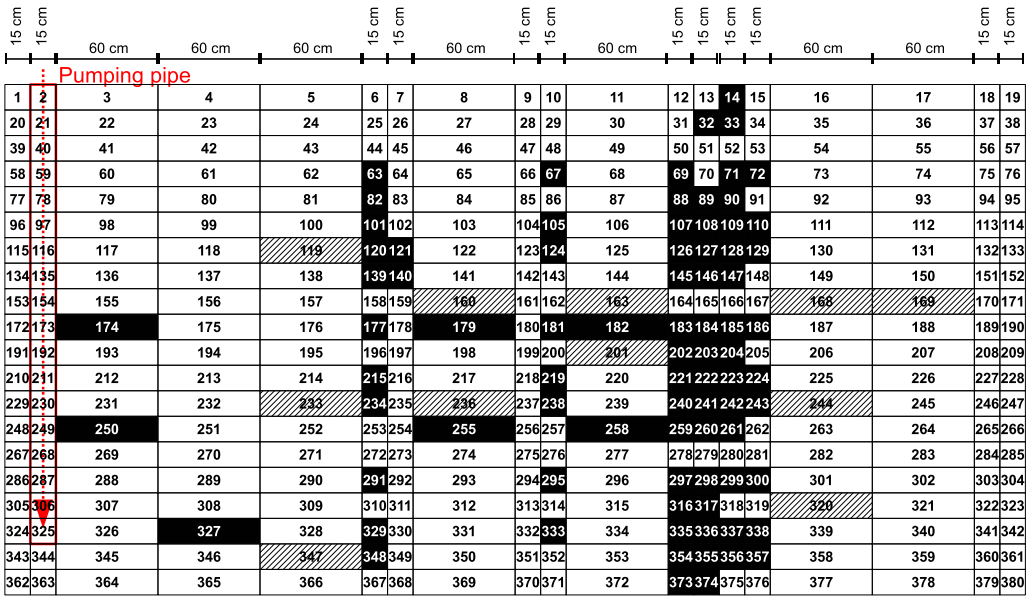

Figure 1: Calibration by magnetic methods on cubic and prismatic specimens (in black) and strength prediction on prismatic specimens (shaded).

3. Experimental procedure

Three uniform continuous coils were used (Fig. 2). The first two coils (Coil 1 and Coil 2) had approximately 8800 turns and a self-inductance of 12.28 and 13.45 H, respectively. The third coil (Coil 3) had fewer turns (approximately 6600) and a reduced inductance of 8.16 H. Contrary to UNE-EN 83512-1, the primary and secondary coils were merged in a unique coil in the three cases. Two impedance analysers were also used, in order to test the different experimental situations. The purpose was to determine their influence on measurement precision. Coil 1 was connected to an Agilent U1732A and Coils 2 and 3 to an LCR 2821A. They were both low-end devices with good accuracy, although the second analyser turned out to be less precise.

Non-uniform continuous coils and discontinuous coils induced a more uniform or an almost constant magnetic field through the coil [30]. The selected coils, however, have a lower magnetic field at the edges. Although the fibres in the central zone of the specimen, along the magnetic flow direction, had a greater weight than those at the end, this behaviour was of relevance in the second part of this study, in which larger prismatic specimens were analysed, which protruded from the coil. The influence on the inductance variation of those parts of the specimen outside the coil will therefore also be lower, thereby obtaining a value for each portion that is much closer to reality.

Following the procedure explained in [16], three measurements were performed on the cubic specimens, with the first device and coil 1: one for each main axis, turning the specimen over and aligning the axis with the magnetic field consecutively (Figures 2b and 2c). The X axis of the specimen is the longitudinal direction within the wall (length), while the Y axis corresponds

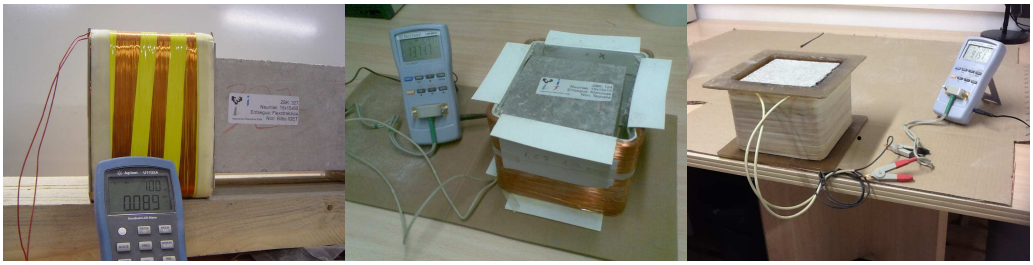

(a) Coil 1 (b) Coil 2 (c) Coil 3

Figure 2: Coils used for testing

to the thickness, and the Z axis is the vertical direction of the wall (height). Thereafter, the average inductance variation was calculated for each specimen. Ferromagnetic elements must be prevented from coming close to the influence area of the magnetic field, as they distort it and give rise to erroneous readings. Depending on the precision of the impedance analyser, one measurement may be sufficient, failing which the average of several successive ones should be calculated. The measurements were repeated for coil 2 and 3 with the second device in those specimens that were not used in the other destructive tests. The objective was to demonstrate proportionality between the measurements.

The prismatic specimens could only be measured on the (longitudinal) X axis, due to the length of the specimen and the configuration of the coil (Figure 2a). Given that the coil was 150 mm high and the prismatic specimen was much larger (600 mm), the measurements were taken with coil 2 in each quarter. In addition to these four measurements, a further two measurements were taken outside the coil, in order to measure the influence on the magnetic field (first and fourth quarters) at the edges of the quarters. Three types of

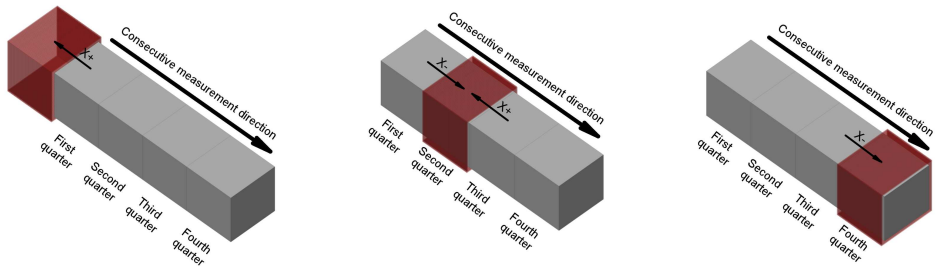

(a) $\Delta L_{x0-,p}$ (b) $\Delta L_{x2,p}$ (c) $\Delta L_{x4,p}$

Figure 3: Measurements in prismatic specimens

influences can be noted among these six measurements. Measurements outside the coil were influenced by the edges of the quarters. The measurements in the first and fourth quarters were increased by the fibre amount of the adjacent quarters. On the other hand, the second and third quarters showed influences from both sides. These three types of influences are shown in Figure 3. Once the prismatic specimens had been tested, they were cut into 4 cubic specimens. Inductance variation was measured on the three axes of these new 28 cubic specimens, as detailed above. Correction factors could therefore be calculated that accounted for the specimen sizes, completing previous studies for cubic ones. The only measurements of interest for the second part of this study were along the X axis.

Measurements in the centre of the specimen, taken on the X axis of coil 2, were used as input data for the strength prediction of the 11 specimens. It is based on a three point bending test on notched prismatic specimens according to UNE-EN 14651. The LOP is obtained as the maximum value reached among those within a range of CMOD < 0.05 mm. The strengths corresponding to the forces applied during the test when the Crack Mouth

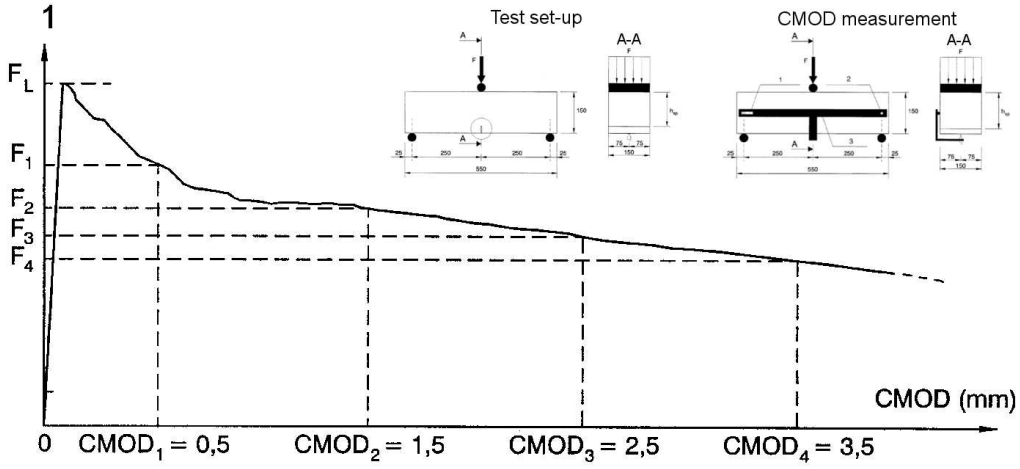

Figure 4: Residual strengths according UNE-EN 14651.

Opening Displacement (CMOD) reaches 0.5, 1.5, 2.5 and 3.5 mm, are considered the successive four residual strengths, as illustrated in Figure 4. Cracks appeared during the bending test in the centre of the specimens, due to weakening caused by the notch. The inductance variation values had to be transformed by the correction factors that were determined to cancel out the influence of the fibres outside the fracture section. These were processed within the range of coil 1, because the prediction was based on data gathered with coil 1.

4. Correction factors

4.1. Cubic specimens

Experimental testing assessed the proportionality of inductance variations. Figure 5 shows the measurements taken from 75 specimens on each of their main axes and their average values. The shape of the lines was

similar in all cases. The age of the concrete in no way altered the measurements. Thus, the concrete showed no ferromagnetic properties whatsoever over time. The remarkably different orientations of the fibres in each specimen were caused by the flow of the self-compacting concrete in the casting process. The pouring point, wall effects and flow direction were the main aspects of this behaviour. As expected, the values along the Y-axis were the smallest and the values for the X-axis were the highest.

The authors have currently conducted a parallel study that attempts to simulate the filling of the formwork by means of computational fluid dynamics (CFD) for comparison of the results with these values.

The concrete flow motion is determined solving the Navier-Stokes equations, for incompressible fluids with a constant viscosity in a multiphase simulation. The Open source Gerris flow solver is used for this homogeneous single fluid approach. The Volume Of Fluid (VOF) technique is also adopted for tracking the interface between concrete and air. The values of the tracer provide the corresponding properties to each phase. A Bingham plastic behaviour is assumed, where the parameters needed have physical sense. Following [31] and [32], such a fluid concrete shows negative values for the yield stress, even though it is physically impossible. Therefore, the rheological parameters adopted in the simulation are a null yield stress (τ_0 = 0 Pa) and a reduced viscosity ($\mu = 63$ Pa $\cdot$ s). The structure is modelled with up to 800, 0.15 meters side boxes. This basic study elements are refined where needed, statically or dynamically, to simulate the advection of the concrete more precisely.

Figure 6 shows the volume of both phases and the interface, for an initial

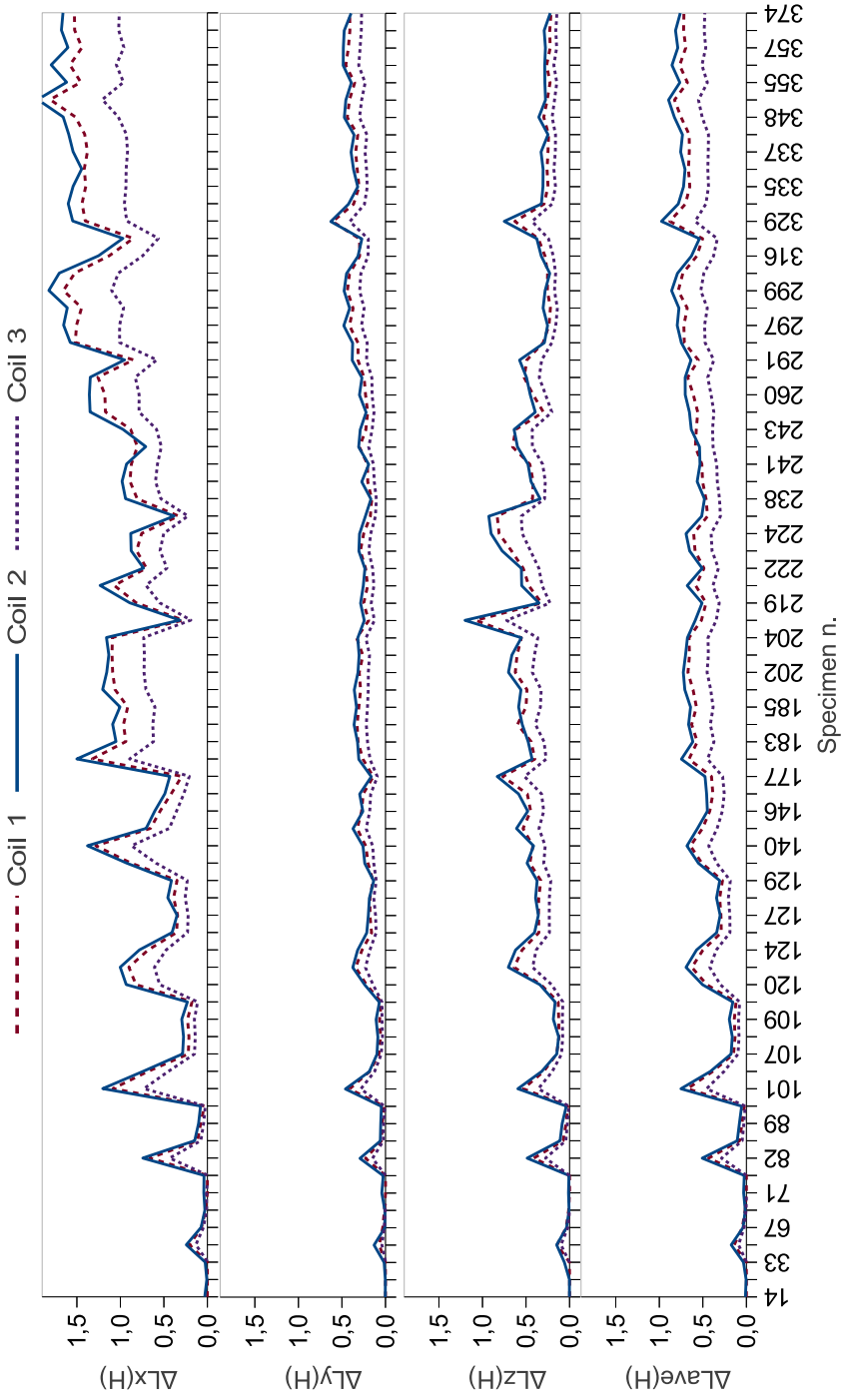

Figure 5: Inductance variations along the three main axes and average values for three different coils.

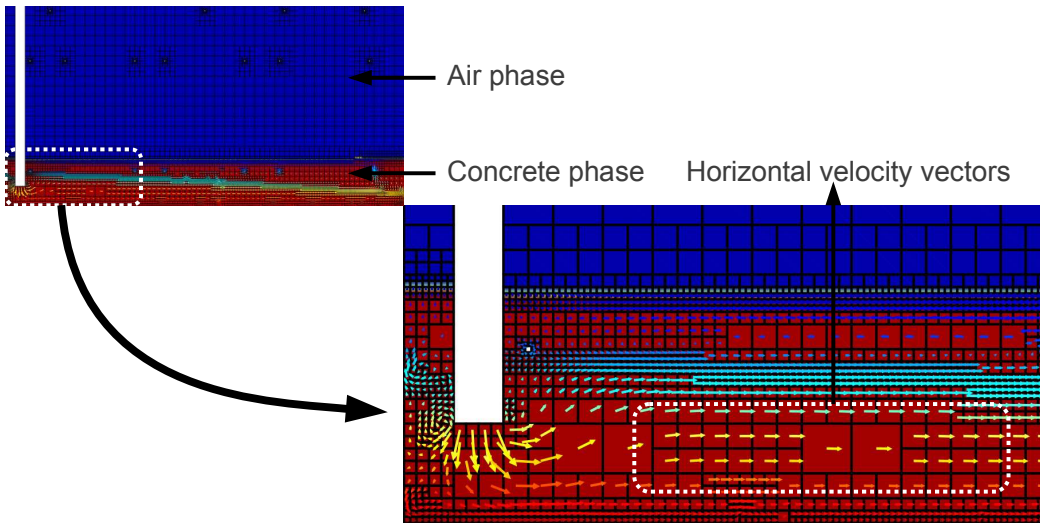

(a) T = 122 s

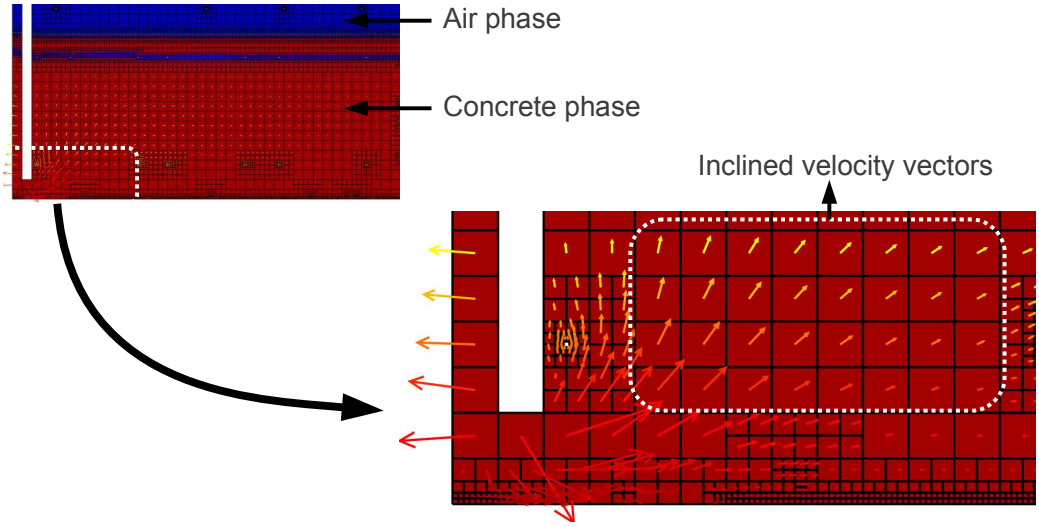

(b) T = 422 s

Figure 6: Initial and final time steps.

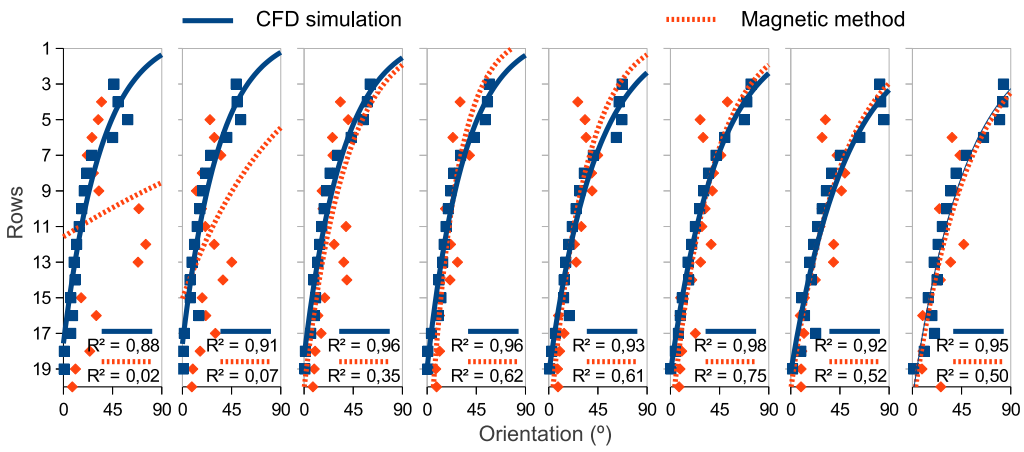

Figure 7: Predicted and detected orientations.

and a final time step. The velocity vectors illustrate the flow direction which vary for each of the elements of the refined mesh. Analysing the development of the vertical and horizontal velocity fields during the whole simulation, and comparing its ratio to the one corresponding to the inductance variation values, ΔL_z and ΔL_x, similar behaviour is obtained in general. Figure 7 represents the orientations predicted by the simulation and the ones detected after applying the magnetic method in the central 8 columns with cubic specimens. The trend in both cases clearly shows the suitability of the prediction tools and the goodness of the magnetic method. The first columns differ from the simulated behaviour, since the removal of the pumping pipe has not been simulated That manoeuvre may have altered the final orientation in those specimens. Since the pipe is lifted with a vertical movement the orientations measured, accordingly, present higher angles than those predicted.

Having established this proportionality, correlations can be presented with established patterns. Taking the measurements of Coil 1 as a cali-

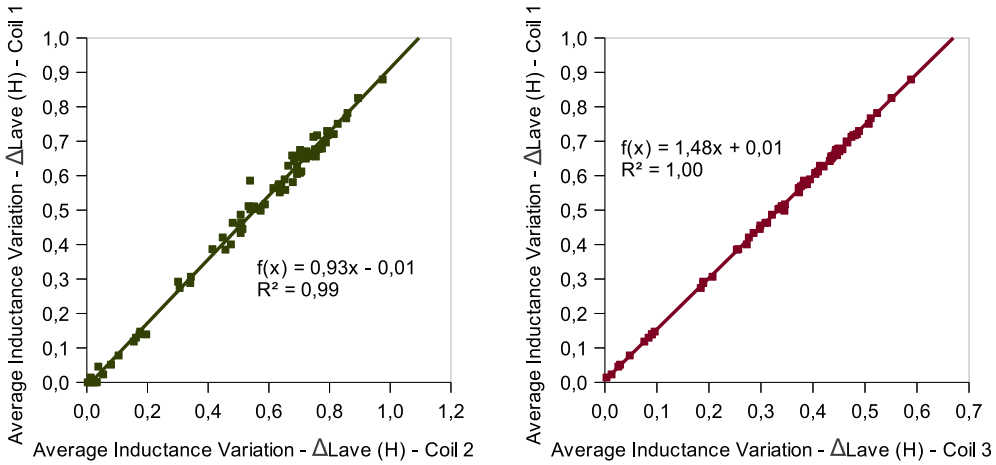

(a) Coil 1 vs coil 2

(b) Coil 1 vs coil 3

Figure 8: Correlation between coils.

bration standard, the data from the linear regression, as shown in Figure 8, were used to transform the values from Coil 2 and Coil 3, with an optimal coefficient of determination in both cases. The slope of the trend line was similar to the division of the self-inductance of both coils. The difference was reduced to a 1.3% for Coil 1 and Coil 2 (Fig. 8a) and to 1.4% for Coil 1 and Coil 3 (Fig. 8b). Due to the lower precision of the second device, a slight scattering was observed in Figure 8a. For that reason, more exhaustive measurements were performed for Coil 3. The oscillation limits of the measurement values were obtained and their average values calculated, the accuracy of which improved (Figure 8b). The difference, however, was not remarkable.

The relevance of the results depends on a comparison of the data with

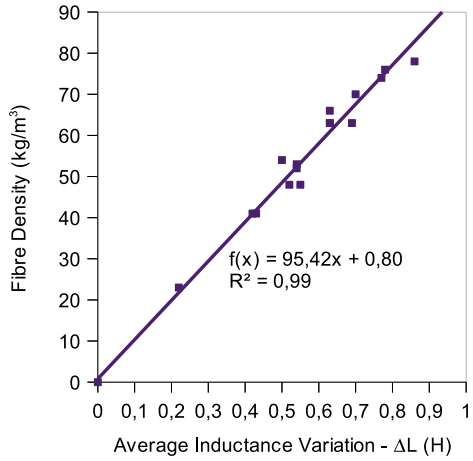

Figure 9: Estimation of fibre density (after [11].

fibre density values. For this type of fibre, inductance variation and the fibre amount was calculated after having crushed some of the specimens from previous studies. The accuracy of the orientation was verified by counting the sectioned fibres on the cut faces and by applying stereological methods as described in [11]. Moreover, the following mechanical tests highlighted the validity of the orientations that were detected. As shown in Figure 9, an average inductance variation of 0.01 H correlated with 1 kg/m^2 of fibre density.

Although the parameters and visual analysis of the slump flow seem correct, the magnetic method shows a noticeable scattering in fibre amount values among the cubic specimens. The simple Volume Of Fluid (VOF) technique adopted in the simulation is not able to detect fibre segregation or asses the dispersing ability of the fibres.

For this reason a Fibre Dynamic Segregation Index (FDSI) is determined

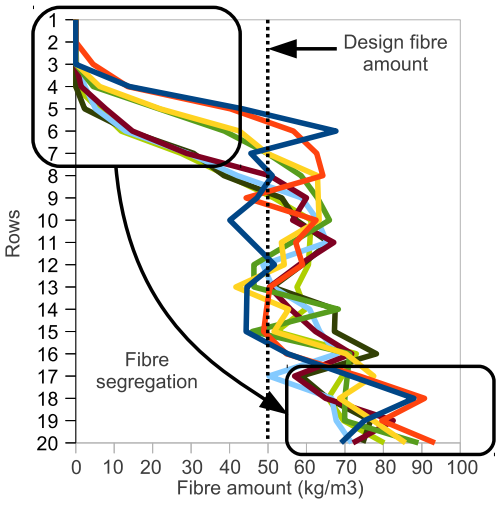

Figure 10: Fibre variation in columns.

for the hardened specimens and analysed as a new methodology proposes [[33]]. This index is obtained as the difference between the fibre amount in the top and the bottom of the wall divided by the mean fibre amount in the column. The central 8 columns with cubic specimens are considered.

Actually there is a severe segregation of fibres in the upper rows, as Figure 10 shows. The study will be divided for the whole wall and for a reduced area where the first 7 rows will be kept apart for a more representative value of the initial concrete mix. It is assumed that the incorrect pumping procedure is responsible of that higher, in absolute values, FDSI.

The high values, in absolute values, obtained can be explained due to, the not so well controlled casting process where, some priming water of the pump was added to the mix. The sensitivity of the mix to water addition is demonstrated in the mentioned methodology. According to it also, initial slump flow values show the proneness to segregation. The vertical directions

Rows	FDSI							
1-20	-1,54	-1,86	-1,81	-1,90	-1,67	-1,73	-1,73	-1,90
8-20	-0.32	-0,46	-0,36	-0,48	-0,35	-0,50	-0,58	-0,66

Table 3: Fibre dynamic segregation indexes.

or columns present great segregation indexes, in absolute values, due to the coupling of static and dynamic segregations during the casting process. Also, the farther the pumping point, the greater the index is.

4.2. Prismatic specimens

The study of 7 specimens before and after cutting followed a procedure to estimate the values of the cubic specimens on the basis of the prismatic ones. The first approach estimated the influence of the part of the specimen that protruded from the coil. Assuming that the magnetic field can also differ slightly from one edge to the other, the influence of fibres outside the coil can also vary. Therefore, two variable influence factors had to be determined. The interaction between the magnetic field and the fibres behind it is denoted by x_-, while x_+ is used for those in front of the coil. $\Delta L_{xi,p}$ and $\Delta L_{xi,c}$ are used to indicate the inductance variation values in both the prismatic and the cubic specimens (cut from prismatic ones), for each of the fourth quarters. Two more measurements were also taken outside the specimen: $\Delta L_{x0-,p}$ on its left and $\Delta L_{x0+,p}$ on its right (Figure 3). The values of the prismatic specimens are known. The values for the cubic specimens were iteratively calculated, until consistent influence factors were established resolving Equation 1.

$$\begin{pmatrix} \Delta L_{x0-,p} \\ \Delta L_{x1,p} \\ \Delta L_{x2,p} \\ \Delta L_{x3,p} \\ \Delta L_{x4,p} \\ \Delta L_{x0+,p} \end{pmatrix} = \begin{pmatrix} 0 & x_+ & 0 & 0 & 0 & 0 \\ 0 & 1 & x_+ & 0 & 0 & 0 \\ 0 & x_- & 1 & x_+ & 0 & 0 \\ 0 & 0 & x_- & 1 & x_+ & 0 \\ 0 & 0 & 0 & x_- & 1 & 0 \\ 0 & 0 & 0 & 0 & x_- & 0 \end{pmatrix} \times \begin{pmatrix} \Delta L_{x0-,c} \\ \Delta L_{x1,c} \\ \Delta L_{x2,c} \\ \Delta L_{x3,c} \\ \Delta L_{x4,c} \\ \Delta L_{x0+,c} \end{pmatrix} \quad (1)$$

The specimens were cut and measured again as described in Section 3 for the cubic specimens, in order to asses the validity of this analytical approach. The measurements were performed with Coil 2 and the values obtained were transformed to Coil 1, as shown in Figure 8a. Figure 11 summarises the inductance variation measurements taken on both the prismatic and the cubic specimens for the analytical as well as the experimental methods. The figure is split in four, one for each quarter of the specimen, depending on the contribution side.

The proposed approach leads to a contribution of the inductance variation of 8% for fibres located in front of the coil and 9% for fibres located behind the coil. In the first quarter, fibres were only located in front of the coil, in the fourth quarter only behind, and the second and the third quarters revealed the influence of the fibres located on both sides. The contribution of fibres outside the coil for the second and third quarters is the sum of the values given above. Similar values were obtained for the experimental method (Figure 11). The slight differences are due to the accumulation of two factors: the thickness of the saw that cuts a small volume of fibres and the small error in the transformation of the values from Coil 2 to Coil 1. Nevertheless, this detracts little or nothing from the accuracy of the values.

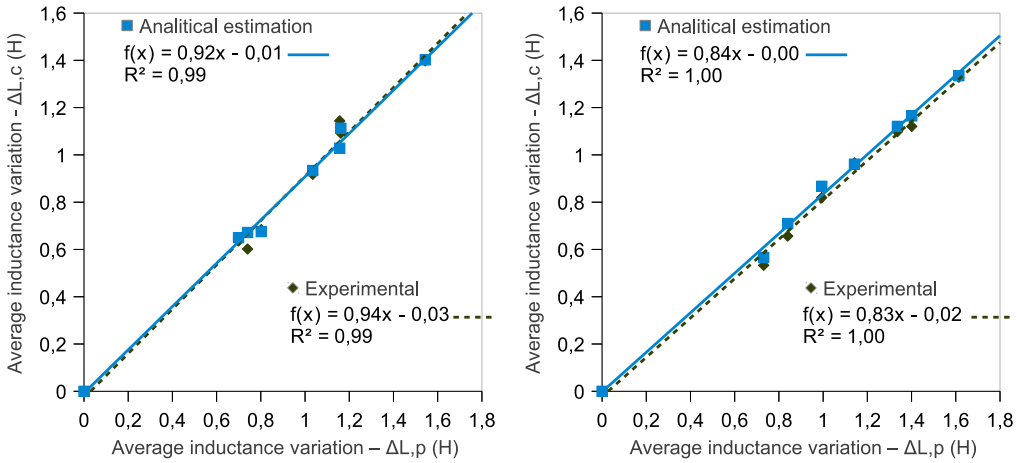

(a) First quarter

(b) Second quarter

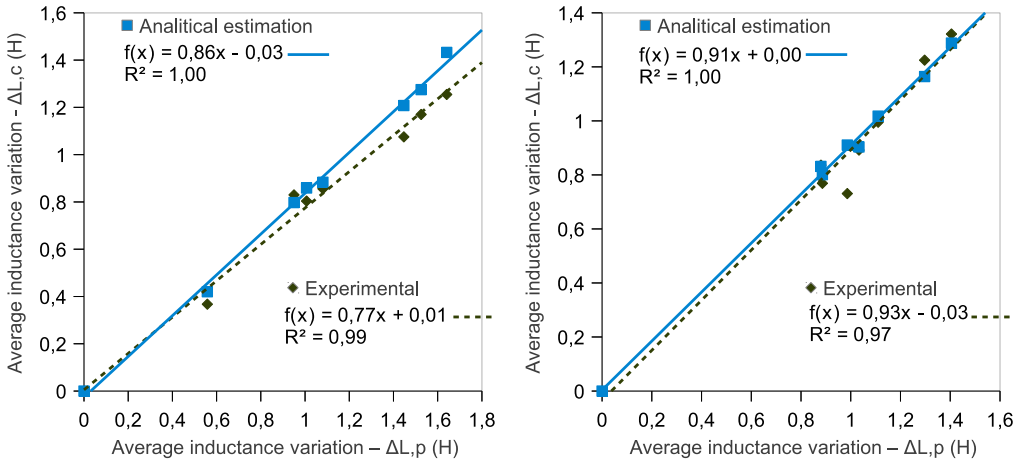

(c) Third quarter

(d) Fourth quarter

Figure 11: Transformation of inductance variations from prismatic specimens to cubic specimens for each quarter.

5. Prediction of strengths

The suitability of the prediction procedure was tested by performing bending tests on 11 new specimens. The key parameters were acquired based on UNE-EN 14651 as the reference standard. The Limit of Proportionality and residual strengths will be anticipated and contrasted with those gathered from the tests. The locations of those specimens, spread throughout out the wall for a representative analysis, are shown in Figure 1.

From previous studies published in [11], some correlations between magnetic and mechanical properties can be estimated. Equations (2a) to (2e) link inductance variation with bending and residual post-cracking strengths. After an inductance variation measurement has been carried out in the centre of each specimen, the values are obtained with the second coil, so they must be transformed to the range of the first coil with the corresponding ratio between both coils. They are also reduced as the influence of the fibres outside the coil is not considered. Concrete reinforcement was indirectly estimated and the different strengths were therefore predicted.

$$f^{f}_{ct,L} = 1.60\Delta L_{centre,p} + 3.61 \tag{2a}$$

$$f_{R,1} = 4.70\Delta L_{centre,p} + 1.03 \tag{2b}$$

$$f_{R,2} = 4.74\Delta L_{centre,p} + 0.79 \tag{2c}$$

$$f_{R,3} = 3.76\Delta L_{centre,p} + 0.76 \tag{2d}$$

$$f_{R,4} = 3.35\Delta L_{centre,p} + 0.30 \tag{2e}$$

Figures 12a to 12e present the result of the bending test together with the predicted values of all the consecutive strengths. As expected, the trend

line of the Limit of Proportionality (LOP) values is less defined than the trend line of the residual strength values. This difference is clearly because the fibres have no notable influence on the tensile strength of the matrix, as their load bearing function is noteworthy after cracking. Therefore, the inductance variation hardly affects the LOP, as can be observed by comparing the slopes of the corresponding trend lines. Instead, the residual strength values show a steeper slope and a greater coefficient of determination (R^2) as well as decreasing parallel trend lines. The tendency is similar to those values used as input for the prediction. The deviation between predicted and real values have multiple causes. The bending test presented some scattering and the values were taken at arbitrarily chosen crack mouth openings. LOP introduces even greater uncertainty, because the highest value reached at a crack opening of up to 0.05 mm was adopted in line with the current standard. Besides, Equations (2a) to (2e) were calculated from the average values of the second and third quarter measurements of the previous specimens, without isolating them from the influence of fibres outside the coil. However, the main drawback is that the coil set-up will have to be further developed to measure the inductance variation of the fibres located in the tensile zone, rather than the whole cross section. High inductance variation values will not necessarily reflect proportional mechanical responses, if the fibres are located in upper or compressed zones of the specimen. The trend lines that are obtained show a moderate increase in their slopes, due to a better approximation of the issue.

Some interesting results may be observed when considering the ratio between predicted and real strength values. Table 4 summarizes those results for all the strengths and their respective average and coefficient of variation

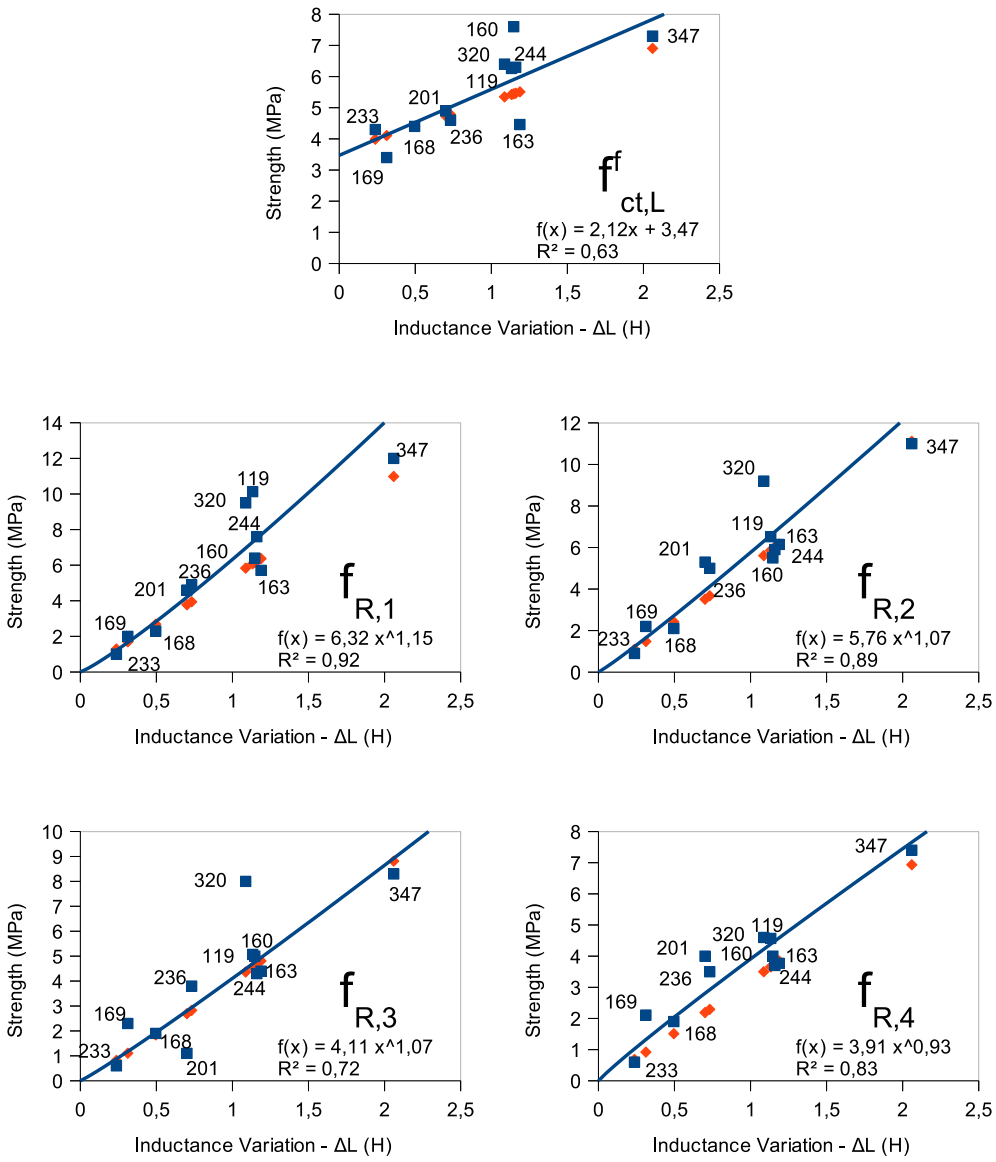

Figure 12: Results from bending test (blue squares) and predicted values (red diamonds).

values. Except for specimen # 233, the values presented are quite close to unity. Specimen # 201 shows a strength drop for the third residual strength, immediately recovering the expected strength values. The above limitations are accentuated for those specimens. Also the average value for each strength is really accurate. Although the coefficients of variation appear high, it must be emphasized that the mechanical behaviour of the wall consists of the sum of the bearing capacity of a wider part that composes it rather than of a isolated small specimen. Consequently, even when there are slightly undervalued areas, there are also others in which the strength is marginally overestimated, matching overall real and predicted behaviours. Those key parameters are, for instance, necessary to obtain the constitutive law of the material, according to the Model Code.

Even though the trend lines of the predicted values (Equations (2a) to (2e)) were not identical to those obtained for the 11 specimens (Figures 12a to 12e) that were tested, the difference was hardly very high at all. Table 5 expressed the inductance variation that should bring each specimen based on the initial and final trend lines, to achieve the strengths determined by the bending tests. Note that the strength corresponding to the Limit of Proportionality has been excluded for not having such a close relation to fibre amount. The average value in most of the specimens is quite similar for both lines. The mean value of the estimated differences is 0.05 Henrys. The coefficients of variation are low enough, except for specimens # 201 and # 233 as mentioned above. It is clearly shown that specimens with low reinforcement aligned with the tensile direction have scattered values. On the other hand, high reinforcements denote high reliability. Fibre amount

Specimen	$f^f_{ct,L}$	$f_{R,1}$	$f_{R,2}$	$f_{R,3}$	$f_{R,4}$
119	0.87	0.63	0.94	0.99	0.90
160	0.72	1.00	1.13	1.01	1.04
163	1.24	1.16	1.04	1.19	1.14
168	1.00	1.46	1.50	1.36	1.03
169	1.21	1.25	1.03	0.84	0.64
201	0.97	0.94	0.78	3.09	0.66
233	0.93	2.14	2.13	2.75	1.82
236	1.04	0.91	0.85	0.92	0.79
244	0.87	0.85	1.07	1.19	1.13
320	0.84	0.65	0.65	0.61	0.86
347	0.95	0.89	0.96	1.02	0.97
Average	0.96	1.08	1.10	1.36	1.00
C.V. (%)	16	40	37	59	32

Table 4: Ratios between predicted strength and real values.

and average inductance variation can be related in Figure 9. Assuming a downward fibre orientation of 50% on the X axis, the approximate average inductance variation for the three main axes should be 0.03 Henrys. This yields an estimation of fibre amounts that differs by about 3 kg/m^3 for each trend line or only a 6% of the design fibre amount of 50 kg/m^3, which may be considered satisfactory.

6. Conclusions

The results of this study have confirmed the potential application of inductive methods for quality control of SFRC. The tests have demonstrated that this non-destructive testing method can determine the orientation and distribution of metallic fibres within the concrete specimens. It is an accurate, simple, and reliable method that can establish patterns for verification due to proportionality between the coils. These patterns, specified by manufacturers and prescribed by national standards, would provide useful information on fibre density as a function of the magnetic properties. Successive measurements can be transformed to the values of calibration standards, multiplying them according to the ratios of self-inductance between the coils. Three different coils were used in the cases under study, of 12.28 H, 13.45 H and 8.16 H. Taking the pattern from the first coil, measurements with the second and third coils can be transformed to the first one, by applying a correction factor of 0.91 and 1.50, respectively. The impedance analysers are capable of accurate and precise measurement of any such variations.

The CFD simulations performed, highlights its potential as a prediction and, therefore, design tool. The orientation trends obtained for a single

Spec.		$f_{R,1}$ (H)	$f_{R,2}$ (H)	$f_{R,3}$ (H)	$f_{R,4}$ (H)	Ave. (H)	C.V. (%)
119	I	1.94	1.21	1.15	1.28	1.39	26
	F	1.59	1.14	1.17	1.22	1.28	16
160	I	1.14	0.99	1.13	1.11	1.09	7
	F	0.99	0.94	1.16	1.05	1.03	9
163	I	0.99	1.13	0.97	1.04	1.03	7
	F	0.88	1.07	1.01	0.97	0.98	8
168	I	0.26	0.27	0.30	0.49	0.33	31
	F	0.34	0.30	0.42	0.39	0.36	14
169	I	0.20	0.31	0.40	0.54	0.36	39
	F	0.29	0.33	0.50	0.45	0.39	25
201	I	0.75	0.95	0.10	1.11	0.72	61
	F	0.70	0.90	0.23	1.05	0.72	50
233	I	-0.02	0.02	-0.03	0.08	0.01	368
	F	0.13	0.08	0.11	-0.03	0.07	96
236	I	0.82	0.89	0.80	0.97	0.87	9
	F	0.75	0.85	0.87	0.90	0.84	8
244	I	1.19	1.08	0.94	1.01	1.06	10
	F	1.03	1.02	0.99	0.94	1.00	4
320	I	1.80	1.77	1.92	1.29	1.69	16
	F	1.48	1.63	1.87	1.24	1.56	17
347	I	2.33	2.14	2.01	2.11	2.15	6
	F	1.88	1.97	1.95	2.10	1.98	5

Table 5: Analysis of the difference between the expected inductance variation for the initial (I) and the final (F) trend lines.

fluid approach, generally, agree with those detected by the magnetic method. However, fibre segregation can not be predicted with this approach.

Post-cracking behaviour can also be indirectly estimated. In the case of the prismatic specimens, a reduction of 8-9% and 14-16% must be applied depending on the portion that is measured, to obtain the real value of each cube. Some calibration patterns could be arranged to relate magnetic and mechanical properties, in order to predict strength values. In this study, it has been proven that inductance variation measurements for 11 prismatic specimens can provide a prediction of mechanical properties and can contribute to better quality control,

Although only small specimens could be measured in the laboratory set-up reported in this study, the tests were in fact non-destructive, because they allowed the specimen to be reused for other tests, i.e. shear strength. This procedure may easily be extrapolated to different fibre types and aspect ratios. Further research is however still needed to develop this interesting method for surface measurements in thin-walled structural elements.

Acknowledgements

The authors gratefully acknowledge the grant obtained from the Spanish Ministry of Science and Innovation through MIVES IV ref: BIA 2010-20789-C04-04 and thank ArcelorMittal-Wire Solutions and Financiera y Minera (Italcementi Group) for materials used in the experimental phase.

They also wish to acknowledge the help of Mr. Ciprian Moldoveanu in performing some of the experimental tests, in partial fulfilment of the requirements for his "BSc" in Civil Engineering at the Military Technical

Academy of Bucarest (Romania)

References

[1] Casanova, P.. Bétons renforcés de fibres métalliques : du matériau la structure. etude expérimentale et analyse du comportement de poutres soumises à la flexion et à l'effort tranchant. Ph.D. thesis; Ecole nationale des ponts et chausses - ENPC PARIS / MARNE LA VALLEE (1995-06-26), P. ROSSI (Dir.). LCPC/BCC - Division Btons et Composites cimentaires; 1995.

[2] Kooiman, A.G.. Modelling steel fibre reinforced concrete for structural design. Ph.D. thesis; Delft University; 2000.

[3] Robins, P., Austin, S., Jones, P.. Pull-out behaviour of hooked steel fibres. Materials and Structures 2002;35:434–442. 10.1007/BF02483148.

[4] Barros, J., Cunha, V., Ribeiro, A., Antunes, J.. Post-cracking behaviour of steel fibre reinforced concrete. Materials and Structures 2005;38:47–56. 10.1007/BF02480574.

[5] Fantilli, A.P., Mihashi, H., Vallini, P.. Multiple cracking and strain hardening in fiber-reinforced concrete under uniaxial tension. Cement and Concrete Research 2009;39(12):1217 – 1229.

[6] Laranjeira, F., Aguado, A., Molins, C., Grnewald, S., Walraven, J., Cavalaro, S.. Framework to predict the orientation of fibers in frc: A novel philosophy. Cement and Concrete Research 2012;42(6):752 – 768.

[7] Stroeven, P.. Stereological principles of spatial modeling applied to steel fiber-reinforced concrete in tension. ACI Materisls Journal 2009;106(3):213 – 222.

[8] Grünewald, S.. Performance-based design of self-compacting fibre reinfroced concrete. Ph.D. thesis; Technische Universiteit Delft; 2004.

[9] Dupont, D., Vandewalle, L.. Distribution of steel fibres in rectangular sections. Cement and Concrete Composites 2005;27(3):391 – 398.

[10] Stähli, P., Custer, R., van Mier, J.. On flow properties, fibre distribution, fibre orientation and flexural behaviour of frc. Materials and Structures 2008;41:189–196. 10.1617/s11527-007-9229-x.

[11] Orbe, A., Cuadrado, J., Losada, R., Rojí, E.. Framework for the design and analysis of steel fiber reinforced self-compacting concrete structures. Construction and Building Materials 2012;35(0):676 – 686.

[12] Roqueta, G., Jofre, L., Romeu, J., Blanch, S.. Broadband propagative microwave imaging of steel fiber reinforced concrete wall structures. Instrumentation and Measurement, IEEE Transactions on 2010;59(12):3102 –3110.

[13] Ozyurt, N., Woo, L.Y., Mason, T.O., Shah, S.P.. Monitoring fiber dispersion in fiber-reinforced cementitious materials: Comparison of ac-impedance spectroscopy and image analysis. ACI Materials Journal 2006;103(5):340–347.

[14] Lataste, J., Behloul, M., Breysse, D.. Characterisation of fibres

distribution in a steel fibre reinforced concrete with electrical resistivity measurements. NDT & E International 2008;41(8):638 – 647.

[15] Van Damme, S., Franchois, A., De Zutter, D., Taerwe, L.. Nondestructive determination of the steel fiber content in concrete slabs with an open-ended coaxial probe. Geoscience and Remote Sensing, IEEE Transactions on 2004;42(11):2511 – 2521.

[16] Torrents, J., Blanco, A., Pujadas, P., Aguado, A., Juan-Garca, P., Snchez-Moragues, M.. Inductive method for assessing the amount and orientation of steel fibers in concrete. Materials and Structures 2012;:1–1610.1617/s11527-012-9858-6.

[17] Blanco, A., Pujadas, P., Aguado, A., Torrents, J.M.. Método inductivo para evaluar cuantía y orientación de fibras de acero en hormigón. In: científico-técnica del hormigón estructural, A., editor. V Congreso de ACHE. Asociación científico-técnica del hormigón estructural; 2011, p. 285–286.

[18] Faifer, M., Ottoboni, R., Toscani, S., Ferrara, L.. Nondestructive testing of steel-fiber-reinforced concrete using a magnetic approach. Instrumentation and Measurement, IEEE Transactions on 2011;60(5):1709 –1717.

[19] Ferrara, L., Faifer, M., Toscani, S.. A magnetic method for non destructive monitoring of fiber dispersion and orientation in steel fiber reinforced cementitious compositespart 1: method calibration. Materials and Structures 2012;45:575–589. 10.1617/s11527-011-9793-y.

[20] Ferrara, L., Faifer, M., Muhaxheri, M., Toscani, S.. A magnetic method for non destructive monitoring of fiber dispersion and orientation in steel fiber reinforced cementitious composites. part 2: Correlation to tensile fracture toughness. MATERIALS AND STRUCTURES 2012;45(4):591–598.

[21] Gettu, R., Gardner, D., Saldivar, H., Barragán, B.. Study of the distribution and orientation of fibers in sfrc specimens. Materials And Structures 2005;38(275):31–37.

[22] Ozyurt, N., Mason, T.O., Shah, S.P.. Correlation of fiber dispersion, rheology and mechanical performance of frcs. Cement and Concrete Composites 2007;29(2):70 – 79.

[23] Torrijos, M., Barragán, B., Zerbino, R.. Physicalmechanical properties, and mesostructure of plain and fibre reinforced self-compacting concrete. Construction and Building Materials 2008;22(8):1780 – 1788.

[24] Torrijos, M.C., Barragán, B.E., Zerbino, R.L.. Placing conditions, mesostructural characteristics and post-cracking response of fibre reinforced self-compacting concretes. Construction and Building Materials 2010;24(6):1078 – 1085.

[25] Martinie, L., Roussel, N.. Simple tools for fiber orientation prediction in industrial practice. Cement And Concrete Research 2011;41(10):993–1000.

[26] Ferrara, L., Tregger, N., Shah, S.P.. Flow-induced fiber orientation in scsfrc: Monitoring and prediction. In: Khayat, K.H., Feys, D., editors.

Design, Production and Placement of Self-Consolidating Concrete; vol. 1 of RILEM Bookseries. Springer Netherlands; 2010, p. 417–428.

[27] Gram, A., Silfwerbrand, J.. Numerical simulation of fresh scc flow: applications. Materials and Structures 2011;44:805–813.

[28] Roussel, N., Geiker, M.R., Dufour, F., Thrane, L.N., Szabo, P.. Computational modeling of concrete flow: General overview. CEMENT AND CONCRETE RESEARCH 2007;37(9):1298–1307.

[29] Thrane, L.N.. Form filling with self-compacting concrete. Ph.D. thesis; Technical University of Denmark; 2007.

[30] Pujadas, P., Blanco, A., de la Fuente, A., Aguado, A.. Cracking behavior of frc slabs with traditional reinforcement. Materials and Structures 2012;45:707–725. 10.1617/s11527-011-9791-0.

[31] Zerbino, R., Barragn, B., Garcia, T., Agull, L., Gettu, R.. Workability tests and rheological parameters in self-compacting concrete. Materials and Structures 2009;42:947–960.

[32] Feys, D., Verhoeven, R., Schutter, G.D.. Evaluation of time independent rheological models applicable to fresh self-compacting concrete. Applied Rheology 2007;17(5):56244–1/56244–10.

[33] Ferrara, L., Bamonte, P., Caverzan, A., Musa, A., Sanal, I.. A comprehensive methodology to test the performance of steel fibre reinforced self-compacting concrete (sfr-scc). Construction and Building Materials 2012;37(0):406 – 424. ¡ce:title¿Non Destructive Techniques for Assessment of Concrete¡/ce:title¿.